RESEARCH ARTICLE

Photodissociation mechanisms of major Hg(II) species in the atmospheric chemical cycle of mercury

Antonio Francés-Monerris,[a,b]† Javier Carmona-García,[c]† A. Ulises Acuña,[d] Juan Z. Dávalos,[d] Carlos A. Cuevas,[d] Douglas E. Kinnison,[e] Joseph S. Francisco,[f] Alfonso Saiz-Lopez*[d] and Daniel Roca-Sanjuán*[c]

Abstract: Mercury is a contaminant of global concern that is transported throughout the atmosphere as elemental mercury Hg(0) and its oxidized forms Hg(I) and Hg(II). The efficient gas phase photolysis of Hg(II) and Hg(I) has recently been reported. However, whether the photolysis of Hg(II) leads to other stable Hg(II) species, to Hg(I), or to Hg(0) and its competition with thermal reactivity are unknown. In this Research article, we show that all oxidized forms of mercury rapidly revert directly and indirectly to Hg(0) via photolysis. Results are based on non-adiabatic dynamics simulations, in which the photoproduct ratios are determined with errors smaller than 3%. We construct for the first time a complete quantitative mechanism of the photochemical and thermal conversion between atmospheric Hg(II), Hg(I), and Hg(0) compounds. These results reveal new fundamental chemistry that has broad implications for the global atmospheric Hg cycle. Thus, photoreduction clearly compete with thermal oxidation being Hg(0) the ultimate fate of Hg in the atmosphere, which significantly increases the lifetime of this metal in the environment.

Introduction

Mercury is an environmental contaminant which once injected to the atmosphere has been found to be dispersed on a global planet-wide scale. It is released into the environment, mainly from present and past industrial activities, essentially in the elemental Hg(0) form. The low chemical reactivity and water solubility of the metal lead to a large atmospheric lifetime (> 6 months) and mobility. Eventually atmospheric mercury is oxidized to water soluble Hg(II) species and deposited on land and waters.[1–5] After deposition into aquatic environments, inorganic mercury can be transformed into methylmercury, a potent neurotoxin harmful to the human population.[6–8]Accordingly, Hg receives a great attention[9–13]

Oxidation of Hg(0) is currently assumed to occur via a single globally-dominant mechanism initiated by photochemically produced atomic bromine (Br), to yield HgBr. Even though earlier schemes considered oxidation by O_3 as the main pathway in the atmosphere,[14] it was later reported that this reaction is irrelevant in the atmosphere since the gas-phase reaction is too slow.[15] Since then, the reaction with very reactive, albeit in low concentration, bromine atoms in the atmosphere is widely assumed to command Hg oxidation globally.[16,17] The radical produced, HgBr, is an intermediate that can then be thermally dissociated back to Hg(0) or further oxidized by atmospheric radicals such as OH, Br, I, Cl, NO_2, HO_2, BrO, IO, and ClO, to form stable Hg(II) compounds.[16,17]

Recently, we have shown that Hg(II)[18] and Hg(I)[19] species efficiently absorb solar radiation and lead to fast photoreduction in the atmosphere. This photoreduction competes with surface deposition, thereby increasing the lifetime and mobility of the metal. However, although Hg(II) photoreduction has been shown to be key in the mercury cycle, the details of the Hg(II) photodissociation reactions and the photoconversion mechanisms among Hg(II), Hg(I), and Hg(0) species at molecular and atomic level remain unknown.

It has been previously suggested that *syn*-HgBrONO and HgBrOOH are the major gaseous oxidized mercury compounds from the reaction of Hg(0) with Br atoms.[3,20,21] Previous computational studies have focused mainly on the thermal reactivity of closed-shell molecules.[6,22–25] Only for *syn*-HgBrONO, a recent computational work[26] indicates that dissociation might occur rapidly in the lower atmosphere giving rise to HgBrO. This radical would further react with atmospheric trace gases, such as NO, NO_2, and volatile organic compounds, to yield finally HgBrOH.[26,27] However, in order to get a comprehensive and quantitative description of the atmospheric Hg chemical mechanism it is required to know the spectral properties and photodissociation reaction products of *syn*-HgBrONO, HgBrOOH, HgBrO and HgBrOH, which are currently unexplored.

† These authors contributed equally.
[a] Dr. A. Francés-Monerris
Université de Lorraine, CNRS, LPCT, F-54000 Nancy, France
[b] Dr. A. Francés-Monerris
Departamento de Química Física, Universitat de València, 46100 Burjassot, Spain.
[c] J. Carmona-García and Dr. Daniel Roca-Sanjuán
Institut de Ciència Molecular, Universitat de València, València 46071, Spain
Daniel.Roca@uv.es
[d] Dr. A. U. Acuña, Dr. J. Z. Dávalos, Dr. C. A. Cuevas and Dr. A. Saiz-Lopez
Department of Atmospheric Chemistry and Climate, Institute of Physical Chemistry Rocasolano, CSIC, Madrid 28006, Spain
a.saiz@csic.es
[e] Dr. D. E. Kinnison
Atmospheric Chemistry Observations and Modelling, NCAR, Boulder, CO 80301, United States
[f] Dr. J. S. Francisco
Department of Earth and Environmental Sciences and Department of Chemistry, University of Pennsylvania, Philadelphia, Pennsylvania 19104, United States

Supporting information for this article is given via a link at the end of the document.

In this Research Article, we report for the first time (i) the UV-vis absorption spectrum, band assignments, and cross section of HgBrO, and (ii) the photo-dissociation channels of *syn*-HgBrONO, HgBrOOH, HgBrO, HgO, and HgBrOH, which are used to deduce the chemical fate of mercury. *Ab initio* non-adiabatic molecular dynamics (AINAMD) with multiconfigurational quantum chemistry is used to determine these important properties. AINAMD is a well-established state-of-the-art tool[28–45] which in this work accounts for the multiconfigurational nature and the strong spin-mixing previously detected in mercury molecules,[46,47] providing an accurate determination of the distinct photo-dissociation yields. Photolysis rates of the mercury compounds listed above are subsequently calculated and incorporated to a kinetic model for the transformations among Hg(II), Hg(I), and Hg(0). This allows to establish the important implications of the photodissociation processes studied here on the atmospheric mercury cycle.

Results and Discussion

The spectra and absorption cross section of *syn*-HgBrONO, HgBrOOH, and HgBrOH, adapted from ref.[18], are shown in Fig. 1 highlighting the spectral region of the electronic transition to the lowest-lying excited state (S_1). This transition is responsible for the major absorption at wavelengths characteristic of the lower troposphere (> 290 nm); smaller contributions from other electronic states are shown in Figs. S1-S3. For *syn*-HgBrONO, two types of transitions of distinct nature originates S_1, i) a mainly monoconfigurational transition, in which the electron excitation is localized in the ONO part of the molecule, occuring from an in-plane oxygen lone pair orbital of the N=O moiety to the anti-bonding π^* orbital (see violet box in Fig. 1a), and ii) a multiconfigurational transition described mainly by the excitation of type i) plus a second excitation in which now the electron departures from an orbital with contributions also from the Hg and Br atoms (delocalized orbital) to the same π^* orbital (see pink box in Fig. 1a). While type i) occurs at the Franck-Condon geometry (band maximum),[26] type ii) appears in other surrounding geometries and contribute to increase the intensity of the S_1 band. Type ii) contributions, from excitations of the HgBr part of the molecule, shall affect the photodynamics of the system, as shown below.

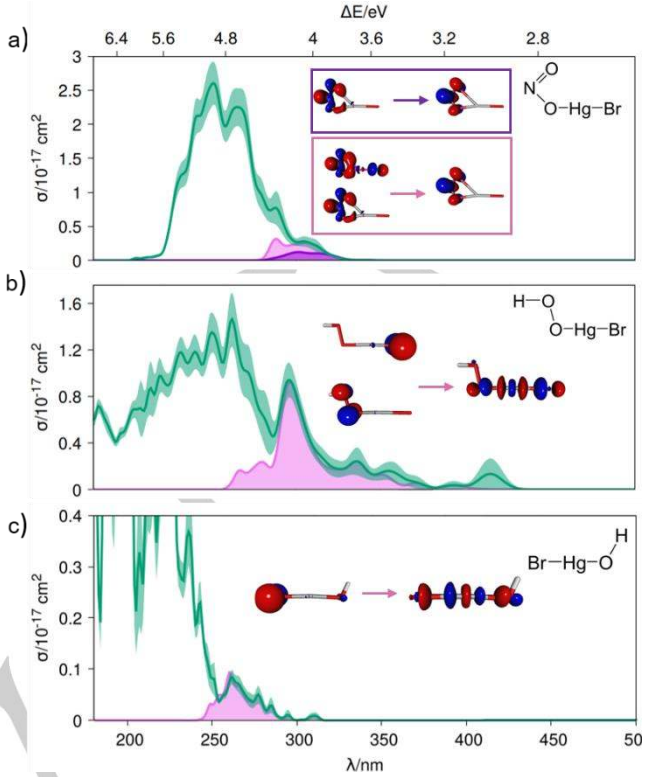

Figure 1. Computed UV-Vis absorption spectra and cross sections (σ/cm^2) of *syn*-HgBrONO, HgBrOOH, and HgBrOH (green curves in a, b, and c, respectively). The green light-colored areas correspond to the uncertainty of the cross section due to the statistical sampling. Pink bands represent the contributions of the lowest-energy excited-state (S_1) to the spectra. The violet band in a) represents only those excitations localized in the ONO moiety (see text). The orbitals that characterize such excited states are also shown. Note the different σ ranges.

In the case of HgBrOOH, the excitation characterizing S_1 is different from that of *syn*-HgBrONO. The electronic density is promoted from lone pair orbitals in Br and O (perpendicular 4p and 2p atomic-like orbitals, respectively) to an anti-bonding σ^* orbital delocalized over the molecule (Fig. 1b), decreasing the strength of Hg-Br and Hg-O bonds. In HgBrOH, similarly to HgBrOOH, the lowest transition implies the population of the σ^* orbital, although in this case the excitation is more dominated by the Br atom (Fig. 1c).

Considering the analysis of the absorption bands, we can conclude that the photodynamics of *syn*-HgBrONO, HgBrOOH, and HgBrOH compounds in the atmosphere must start from the S_1 electronic state. This state shows no energy barriers neither along the Hg-O dissociation coordinate nor along the Hg-Br bond stretching (see two-dimensional potential energy surfaces (2D-PES) in Figs. S10-S12 and Tables S3-S14 This indicates that dynamical effects and interaction between the ground and excited electronic states (non-adiabatic and spin-orbit couplings) would be key factors to determine the branching ratio between the photoproducts. AINAMD performed for the three compounds after absorption to the lowest-energy band reveals an ultrafast decay

of the initial S_1 state in *ca.* a tenth of picosecond, populating nearby singlet and triplet states (Figs. S22-S24).

Analysis of the bond distances along the dynamic processes reveals the distinct photodissociation channels and the corresponding photoproduct yields, which are summarized in Fig. 2. The photodissociation of *syn*-HgBrONO is relatively simple in terms of the number of photoproducts that have been identified in the AINAMD simulations. Most (90%) of the trajectories lead to ejection of nitric oxide thus forming the HgBrO radical (Fig. S26 and Table S27). The rest of trajectories (10%) yield HgBr upon release of NO_2. These results confirm previous CCSD(T) estimations which point to HgBrO as the main photoproduct.[26] However, the present dynamical calculations allow to predict the specific yield of every reaction channel. The predominance of the HgBrO photoproduct is due to the localized excitation taking place in the ONO part of the molecule (Fig. 1a), since the population of the anti-bonding π^* of the ONO group favors the HgBrO-NO bond breaking. The formation of HgBr can be related to the other excitations delocalized over the whole molecule.

For HgBrOOH and HgBrOH, three major types of photodissociation channels have been identified, as the result of the Hg-Br, Hg-O, and O-O bond cleavages (Figures 2 and S27-S28 and Tables S28-S29). The first dominant channel (66 and 49% for HgBrOOH and HgBrOH, respectively) simultaneously breaks both Hg-Br and Hg-O bonds, yielding atomic bromine and mercury. The second most important photoreaction (31%) for HgBrOOH is O-O bond cleavage to yield HgBrO radical (+ OH), as in *syn*-HgBrONO, while for HgBrOH, formation of this radical is negligible (1%). In contrast, the second channel (35%) in this last case corresponds to Hg-Br bond breaking producing HgOH radical, probably due to the more dominant presence of Br in the HgBrOH excitation (Fig. 1c). Thirdly, the photon excitation energy may also dissociate the Hg-O bond while preserving Hg-Br bonding, this being more probable in HgBrOH (15%) than in HgBrOOH. In this last compound, the photoproducts are HgBr + O + OH (~2 %) and HgBr + OOH (<1 %). Finally, note that HgO molecules can also be obtained by photolysis of HgBrOOH in a very low yield (<1 %).

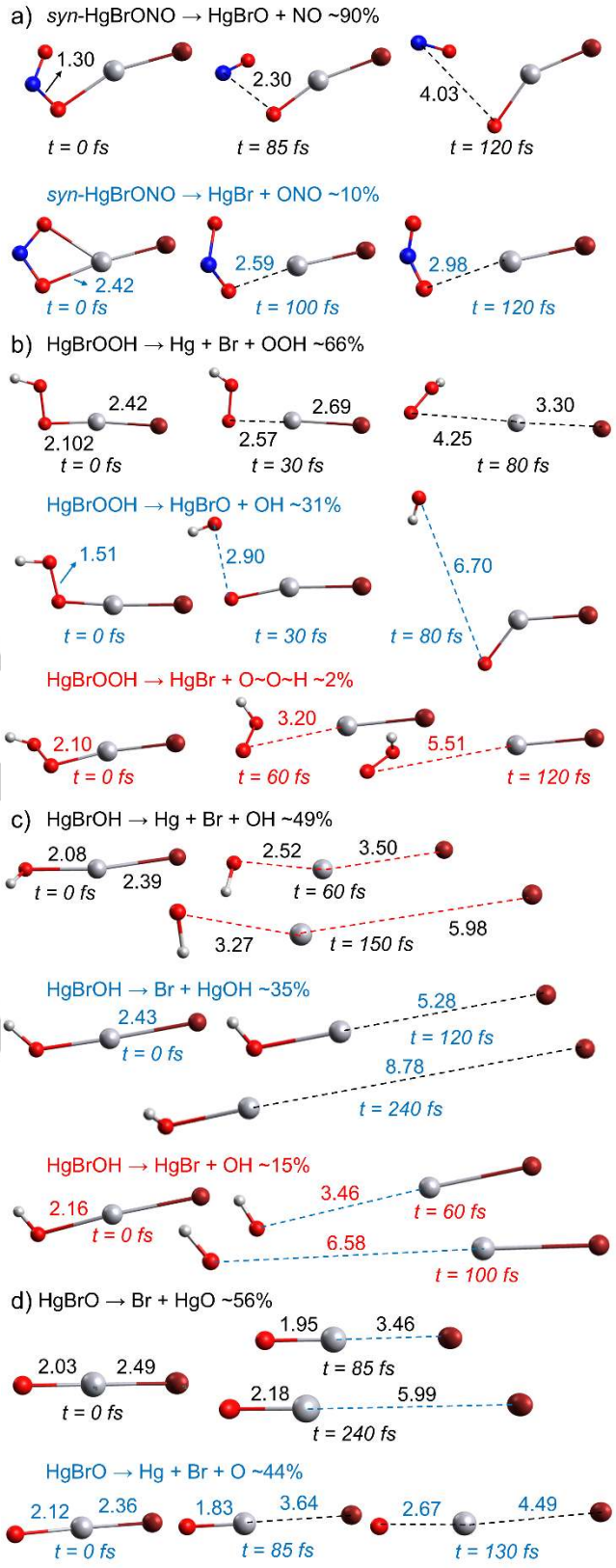

Figure 2. Main photodissociation channels of a) *syn*-HgBrONO, b) HgBrOOH, c) HgBrOH, and d) HgBrO resulting from light absorption to the atmospherically-

relevant electronic excited-state. Panels show selected snapshots of archetypical trajectories. Distances in Å.

The HgBrO radical appears as an important product in the photolysis of *syn*-HgBrONO and HgBrOOH and it has been suggested to further react with NO, NO_2, and volatile organic compounds within the lower troposphere to yield HgBrONO, $HgBrONO_2$, and HgBrOH, respectively.[26] On the other hand, the UV-Vis absorption spectrum and photochemical properties of this radical remain unknown. The spectrum and absorption cross sections are shown in Fig.3, indicating the contribution of the lowest excited states as before (additional details in Fig. S4). Two bands appear in the atmospheric region (300-500 nm) related to the electronic transitions from the ground (D_1) to the fourth (D_4) and fifth (D_5) electronic states. In addition, a lower intensity band shows at ~650 nm corresponding to the excitation to the third state (D_3). The D_1 unpaired electron in the 2p orbitals of the O atom relocates to the Br atom 4p orbitals on excitation to D_4 and D_5 (Fig. 3). Single or double dissociation reactions leading to Hg(I) or Hg(0), respectively, are energetically accessible (see 2D-PES in Fig. S13 and Tables S15-S18).

In contrast to *syn*-HgBrONO and HgBrOOH, where day-light absorption is dominated by the lowest excited state (S_1), in HgBrO three excited doublet states below 3.5 eV can be potentially populated. Therefore, the three of them were considered as initial states in the photodynamic simulations,[48] as described in the SI. Our computations show a femtosecond depopulation to the lowest-lying degenerate states (Fig. S20), while the analysis of the Hg-Br and Hg-O distances of the ensemble of trajectories (Fig. S29, Table S30), reveals two main photoproducts: HgO (56%) and Hg(0) (44%) (Fig. 2d), being Hg-Br the most photolabile bond of the radical.

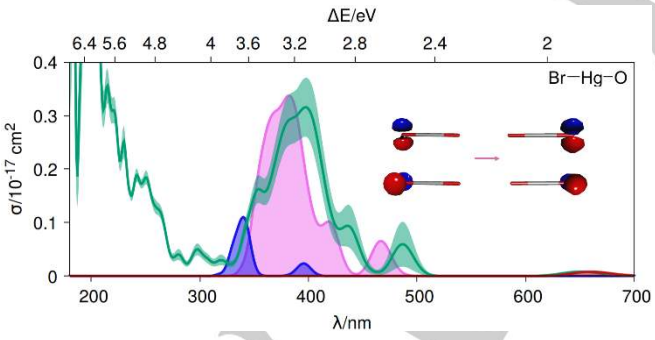

Figure 3. UV-Vis absorption spectra and cross sections (σ/cm^2) of HgBrO radical (green curve). The green light areas correspond to the uncertainty of the cross section due to statistical sampling. Red, pink, and blue bands represent the contributions of the lowest-energy doublet excited states (D_3, D_4, and D_5, respectively) to the spectra. The orbitals that characterize such excited states are also shown.

The HgBr, HgOH, and HgO radicals are generated in the present photodynamics. HgBr and HgOH were found in our previous work to further dissociate to Hg(0) upon absorption to the electronic states in the energy range 500-800 nm, while a clearly bound excited state was determined with an absorption band appearing at 300-400 nm.[19] In the case of mercury oxide HgO, our previous calculation of the absorption spectrum[18] revealed absorption bands at 290-320 and 350-400 nm for the $^1\Sigma$ and $^3\Pi$ states, respectively. The potential energy curves computed in this work show favorable dissociation channels to yield Hg(0) (Fig. S14).

To assess the atmospheric impact of these results, we use the global chemistry–climate model CAM-Chem[49] to estimate the photolysis rates (J/s^{-1}) of oxidized Hg species, as described elsewhere[18] and detailed in section 6 of the SI. Fig. 4 shows the computed probability for the different photodissociation channels (in red) and the photolysis and pseudo-first order rates (in black) computed herein or taken from the literature (see also Table S35). *syn*-HgBrONO photodissociates to HgBrO (90%) and HgBr (10%) while HgBrOOH breaks down to HgBrO (31%) and directly to Hg(0) (66%). The absorption cross-section of HgBrO in the 290-550 nm range results in a global tropospheric photolysis rate of 2.95×10^{-2} s^{-1}. Therefore, the photolysis of HgBrO cannot compete with its recently reported reaction with methane (k'=11 s^{-1} at 298K and 1 atm).[26] Nevertheless, the reaction with methane produces HgBrOH, which has a short photolytic lifetime of ~1 day[18] and will regenerate Hg(0) directly or indirectly through HgBr and HgOH, as shown herein (Fig. 4). We calculate that the photolysis of the major Hg(II) species (*syn*-HgBrONO, HgBrOOH, and HgBrOH summed together, see Tables S27-S29) leads to Hg(0) directly (39%), and indirectly (61%) via intermediate radicals of short photolytic lifetime. These results show Hg(0) as the net predominant photoproduct of Hg(II) photolysis, which significantly increases the atmospheric mercury lifetime.

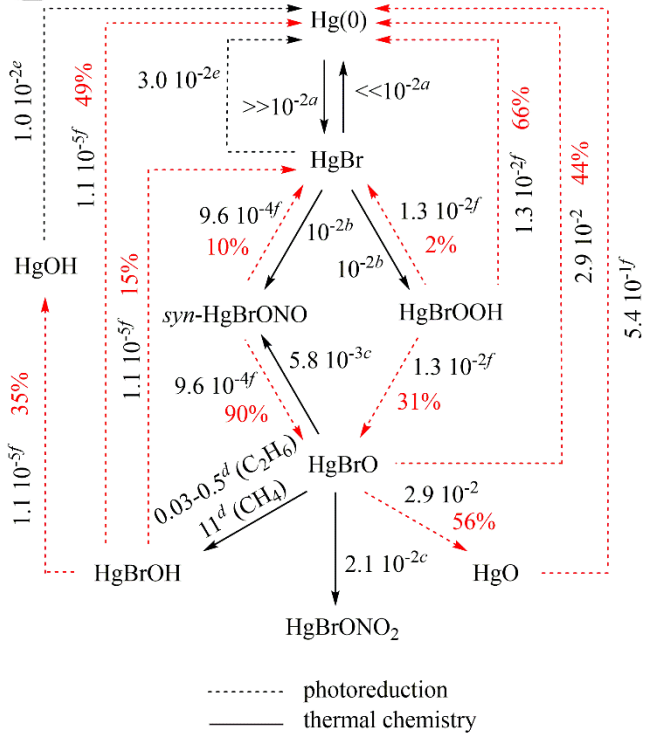

Figure 4. Quantitative kinetic model and rates (s^{-1}) for the atmospheric photochemistry of major Hg species. Photodissociation channels computed in this work are shown in red arrows and the corresponding yields in red percentages. [a]Ref.[16] [b]Ref.[50] [c]pseudo-first order rates according to $k(HgBrO+NO)=2.9\times10^{-11}$ cm^3 $molec^{-1}$ s^{-1},[26] tropospheric averaged concentration of NO of 1.99×10^8 molec cm^{-3}, and $k(HgBrO+NO_2)=1.7\times10^{-11}$ cm^3 $molec^{-1}$ s^{-1},[26] tropospheric averaged concentration of NO_2 of 1.25×10^9 molec cm^{-3}. [d]Ref. [26] [e]Ref. [19] [f]Ref. [18].

Conclusion

Day-light solar absorption photo-reduces all oxidized forms of mercury, *syn*-HgBrONO, HgBrOOH, and HgBrOH, to Hg(0) directly in the femtosecond scale or indirectly via the HgBrO, HgO, HgBr, or HgOH intermediate species. This rich and novel photodissociation processes of Hg(II) species uncovered here have broad implications for the chemical mechanisms determining the atmospheric mercury residence time and its global dispersion. Overall, this new fundamental information also provides for the first time a complete quantitative mechanism of the photoconversion between Hg(II), Hg(I), and Hg(0) species in the atmosphere.

Computational Details

Cross sections were computed using the complete-active-space self-consistent field (CASSCF) method assisted by the multistate complete-active-space second-order perturbation theory (MS-CASPT2)[51–54] methodology and Wigner nuclear sampling. Photodissociation yields and decay lifetimes were computed with AINAMD incorporating spin-orbit coupling (SOC) with and the surface-hoping including arbitrary couplings (SHARC) scheme,[55,56] as implemented in the coupled OpenMolcas[57,58] and SHARC 2.0[59,60] programs. Analysis of the standard deviations considering different sets of trajectories indicates that the photoproduct ratios are determined with errors below 3%. Photolysis rates were calculated using the global chemistry–climate model CAM-Chem.[49] The reader is referred to the Supporting Information for further details on the static and dynamic calculations and Tables S1-S35 and Figures S1-S29 for additional data.

Acknowledgements

This work was supported by the MINECO/FEDER through Project No. CTQ2017-87054-C2-2-P and the Consejo Superior de Investigaciones Cientificas (CSIC) of Spain. A.F.-M. is grateful to the Generalitat Valenciana and the European Social Fund for the postdoctoral contract (APOSTD/2019/149). D.R.-S. is thankful to the Spanish MINECO/FEDER also for financial support through the Ramon y Cajal fellowship with ref. RYC- 2015-19234, and the Unit of Excellence Maria de Maeztu MDM-2015-0538. This study has received funding from the European Research Council Executive Agency under the European Union´s Horizon 2020 Research and Innovation programme (Project ERC-2016-COG 726349 CLIMAHAL).

Keywords: Hg atmospheric chemical cycle • ab initio non-adiabatic molecular dynamics • CASSCF/CASPT2 • photodissociation • global chemistry climate model

[1] E. G. Pacyna, J. M. Pacyna, K. Sundseth, J. Munthe, K. Kindbom, S. Wilson, F. Steenhuisen, P. Maxson, *Atmos. Environ.* **2010**, *44*, 2487–2499.

[2] D. G. Streets, H. M. Horowitz, D. J. Jacob, Z. Lu, L. Levin, A. F. H. ter Schure, E. M. Sunderland, *Environ. Sci. Technol.* **2017**, *51*, 5969–5977.

[3] H. M. Horowitz, D. J. Jacob, Y. Zhang, T. S. Dibble, F. Slemr, H. M. Amos, J. A. Schmidt, E. S. Corbitt, E. A. Marais, E. M. Sunderland, *Atmos. Chem. Phys.* **2017**, *17*, 6353–6371.

[4] F. Wang, A. Saiz-Lopez, A. S. Mahajan, J. C. Gómez Martín, D. Armstrong, M. Lemes, T. Hay, C. Prados-Roman, *Atmos. Chem. Phys.* **2014**, *14*, 1323–1335.

[5] D. G. Streets, H. M. Horowitz, Z. Lu, L. Levin, C. P. Thackray, E. M. Sunderland, *Atmos. Environ.* **2019**, *201*, 417–427.

[6] P. A. Ariya, M. Amyot, A. Dastoor, D. Deeds, A. Feinberg, G. Kos, A. Poulain, A. Ryjkov, K. Semeniuk, M. Subir, et al., *Chem. Rev.* **2015**, *115*, 3760–3802.

[7] Unep, *United Nations Environment Programme Global Mercury Assessment 2013 Sources, Emissions, Releases and Environmental Transport*, **n.d.**

[8] A. T. Schartup, C. P. Thackray, A. Qureshi, C. Dassuncao, K. Gillespie, A. Hanke, E. M. Sunderland, *Nature* **2019**, *572*, 648–650.

[9] S. Yoon, E. W. Miller, Q. He, P. H. Do, C. J. Chang, *Angew. Chemie - Int. Ed.* **2007**, *46*, 6658–6661.

[10] P. Donati, M. Moglianetti, M. Veronesi, M. Prato, G. Tatulli, T. Bandiera, P. P. Pompa, *Angew. Chemie - Int. Ed.* **2019**, DOI 10.1002/anie.201905669.

[11] M. Mon, F. Lloret, J. Ferrando-Soria, C. Martí-Gastaldo, D. Armentano, E. Pardo, *Angew. Chemie - Int. Ed.* **2016**, *55*, 11167–11172.

[12] Z. H. Lin, G. Zhu, Y. S. Zhou, Y. Yang, P. Bai, J. Chen, Z. L. Wang, *Angew. Chemie - Int. Ed.* **2013**, *52*, 5065–5069.

[13] B. C. Ye, B. C. Yin, *Angew. Chemie - Int. Ed.* **2008**, *47*, 8386–8389.

[14] J. G. Calvert, S. E. Lindberg, *Atmos. Environ.* **2005**, *39*, 3355–3367.

[15] A. J. Hynes, D. L. Donohoue, M. E. Goodsite, I. M. Hedgecock, in *Mercur. Fate Transp. Glob. Atmos.*, Springer US, Boston, MA, **2009**, pp. 427–457.

[16] M. E. Goodsite, J. M. C. Plane, H. Skov, *Environ. Sci. Technol.* **2004**, *38*, 1772–1776.

[17] C. D. Holmes, D. J. Jacob, E. S. Corbitt, J. Mao, X. Yang, R. Talbot, F. Slemr, *Atmos. Chem. Phys* **2010**, *10*, 12037–12057.

[18] A. Saiz-Lopez, S. P. Sitkiewicz, D. Roca-Sanjuán, J. M. Oliva-Enrich, J. Z. Dávalos, R. Notario, M. Jiskra, Y. Xu, F. Wang, C. P. Thackray, et al., *Nat. Commun.* **2018**, *9*, 4796.

[19] A. Saiz-Lopez, A. U. Acuña, T. Trabelsi, J. Carmona-García, J. Z. Dávalos, D. Rivero, C. A. Cuevas, D. E. Kinnison, S. P. Sitkiewicz, D. Roca-Sanjuán, et al., *J. Am. Chem. Soc.* **2019**, *141*, 8698–8702.

[20] T. S. Dibble, M. J. Zelie, H. Mao, *Atmos. Chem. Phys* **2012**, *12*, 10271–10279.

[21] T. S. Dibble, A. C. Schwid, *Chem. Phys. Lett.* **2016**, *659*, 289–294.

[22] G. Ohanessian, M. J. Brusich, W. A. Goddard, *J. Am. Chem. Soc.*

1990, *112*, 7179–7189.

[23] L. Si, P. A. Ariya, *Environ. Sci. Technol.* **2008**, *42*, 5150–5155.

[24] M. Kaupp, H. G. von Schnering, *Angew. Chemie Int. Ed. English* **1993**, *32*, 861–863.

[25] L. Yue, S. Zhou, X. Sun, M. Schlangen, H. Schwarz, *Angew. Chemie - Int. Ed.* **2018**, *57*, 3251–3255.

[26] K. T. Lam, C. J. Wilhelmsen, A. C. Schwid, Y. Jiao, T. S. Dibble, *J. Phys. Chem. A* **2019**, *123*, 1637–1647.

[27] N. B. Balabanov, K. A. Peterson, *J. Phys. Chem. A* **2003**, *107*, 7465–7470.

[28] C. Rauer, J. J. Nogueira, P. Marquetand, L. González, *J. Am. Chem. Soc.* **2016**, *138*, 15911–15916.

[29] Z. Zhou, J. Liu, R. Long, L. Li, L. Guo, O. V. Prezhdo, *J. Am. Chem. Soc.* **2017**, *139*, 6707–6717.

[30] M. Nazari, C. D. Bösch, A. Rondi, A. Francés-Monerris, M. Marazzi, E. Lognon, M. Gazzetto, S. M. Langenegger, R. Häner, T. Feurer, et al., *Phys. Chem. Chem. Phys.* **2019**, *21*, 16981–16988.

[31] G. Cui, W. Thiel, *Angew. Chemie - Int. Ed.* **2013**, *52*, 433–436.

[32] S. Essafi, D. P. Tew, J. N. Harvey, *Angew. Chemie - Int. Ed.* **2017**, *56*, 5790–5794.

[33] Y. Lu, Z. Lan, W. Thiel, *Angew. Chemie - Int. Ed.* **2011**, *50*, 6864–6867.

[34] D. Morozov, G. Groenhof, *Angew. Chemie - Int. Ed.* **2016**, *55*, 576–578.

[35] M. Böckmann, N. L. Doltsinis, D. Marx, *Angew. Chemie - Int. Ed.* **2010**, *49*, 3382–3384.

[36] A. Valentini, D. Rivero, F. Zapata, C. García-Iriepa, M. Marazzi, R. Palmeiro, I. Fdez. Galván, D. Sampedro, M. Olivucci, L. M. Frutos, *Angew. Chemie - Int. Ed.* **2017**, *56*, 3842–3846.

[37] D. Polli, O. Weingart, D. Brida, E. Poli, M. Maiuri, K. M. Spillane, A. Bottoni, P. Kukura, R. A. Mathies, G. Cerullo, et al., *Angew. Chemie - Int. Ed.* **2014**, *53*, 2504–2507.

[38] S. A. Fischer, W. R. Duncan, O. V. Prezhdo, *J. Am. Chem. Soc.* **2009**, *131*, 15483–15491.

[39] R. Borrego-Varillas, D. C. Teles-Ferreira, A. Nenov, I. Conti, L. Ganzer, C. Manzoni, M. Garavelli, A. Maria de Paula, G. Cerullo, *J. Am. Chem. Soc.* **2018**, *140*, 16087–16093.

[40] P. Mondal, G. Granucci, D. Rastädter, M. Persico, I. Burghardt, *Chem. Sci.* **2018**, *9*, 4671–4681.

[41] L. Martínez-Fernández, I. Corral, G. Granucci, M. Persico, *Chem. Sci.* **2014**, *5*, 1336.

[42] T. W. Kim, S. Jun, Y. Ha, R. K. Yadav, A. Kumar, C.-Y. Yoo, I. Oh, H.-K. Lim, J. W. Shin, R. Ryoo, et al., *Nat. Commun.* **2019**, *10*, 1873.

[43] S. Mai, M. Pollum, L. Martínez-Fernández, N. Dunn, P. Marquetand, I. Corral, C. E. Crespo-Hernández, L. González, *Nat. Commun.* **2016**, *7*, 13077.

[44] M. Barbatti, A. J. A. Aquino, J. J. Szymczak, D. Nachtigallová, P. Hobza, H. Lischka, *Proc. Natl. Acad. Sci. U. S. A.* **2010**, *107*, 21453–8.

[45] D. Polli, P. Altoè, O. Weingart, K. M. Spillane, C. Manzoni, D. Brida, G. Tomasello, G. Orlandi, P. Kukura, R. A. Mathies, et al., *Nature* **2010**, *467*, 440–443.

[46] S. P. Sitkiewicz, J. M. Oliva, J. Z. Dávalos, R. Notario, A. Saiz–Lopez, D. R. Alcoba, O. B. Oña, D. Roca-Sanjuán, *J. Chem. Phys.* **2016**, *145*, 244304.

[47] S. Sitkiewicz, D. Rivero, J. M. Oliva, A. Saiz-Lopez, D. Roca-Sanjuán, *Phys. Chem. Chem. Phys.* **2018**, *21*, 455–467.

[48] M. Barbatti, G. Granucci, M. Ruckenbauer, F. Plasser, J. Pittner, M. Persico, H. Lischka, *Max-Planck-Institut für Kohlenforsch. Mülheim an der Ruhr, Ger.* **2011**.

[49] J.-F. Lamarque, L. K. Emmons, P. G. Hess, D. E. Kinnison, S. Tilmes, F. Vitt, C. L. Heald, E. A. Holland, P. H. Lauritzen, J. Neu, et al., *Geosci. Model Dev.* **2012**, *5*, 369–411.

[50] Y. Jiao, T. S. Dibble, *Phys. Chem. Chem. Phys.* **2017**, *19*, 1826–1838.

[51] K. Andersson, P. Å. Malmqvist, B. O. Roos, A. J. Sadlej, K. Wolinski, *J. Phys. Chem.* **1990**, *94*, 5483–5488.

[52] K. Andersson, P. Malmqvist, B. O. Roos, *J. Chem. Phys.* **1992**, *96*, 1218–1226.

[53] J. Finley, P. Å. Malmqvist, B. O. Roos, L. Serrano-Andrés, *Chem. Phys. Lett.* **1998**, *288*, 299–306.

[54] D. Roca-Sanjuán, F. Aquilante, R. Lindh, *Wiley Interdiscip. Rev. Comput. Mol. Sci.* **2012**, *2*, 585–603.

[55] S. Mai, P. Marquetand, L. González, *Int. J. Quantum Chem.* **2015**, *115*, 1215–1231.

[56] M. Richter, P. Marquetand, J. González-Vázquez, I. Sola, L. González, *J. Chem. Theory Comput.* **2011**, *7*, 1253–1258.

[57] F. Aquilante, J. Autschbach, R. K. Carlson, L. F. Chibotaru, M. G. Delcey, L. De Vico, I. Fdez. Galván, N. Ferré, L. M. Frutos, L. Gagliardi, et al., *J. Comput. Chem.* **2016**, *37*, 506–541.

[58] I. F. Galván, M. Vacher, A. Alavi, C. Angeli, J. Autschbach, J. J. Bao, S. I. Bokarev, N. A. Bogdanov, R. K. Carlson, L. F. Chibotaru, et al., *J. Chem. Theor. Comput* **2019**, *15*, 5925–5964.

[59] S. Mai, M. Richter, M. Heindl, M. F. S. J. Menger, A. Atkins, M. Ruckenbauer, F. Plasser, M. Oppel, P. Marquetand, L. González, **2018**, sharc-md.org.

[60] S. Mai, P. Marquetand, L. González, *Wiley Interdiscip. Rev. Comput. Mol. Sci.* **2018**, *8*, e1370.

Entry for the Table of Contents

RESEARCH ARTICLE

Photoconversion dynamics between atmospheric Hg(0), Hg(I), and Hg(II) species show that the ultimate fate of this metal in the atmosphere is elemental Hg.

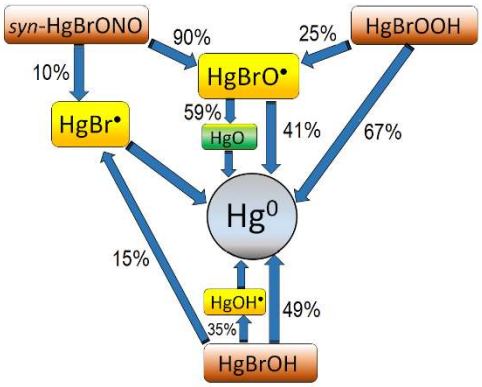

A. Francés-Monerris, J. Carmona-García, A. U. Acuña, J. Z. Dávalos, C. A. Cuevas, D. E. Kinnison, J. S. Francisco, A. Saiz-Lopez and D. Roca-Sanjuán**

Page No. – Page No.
Photodissociation mechanisms of major Hg(II) species in the atmospheric chemical cycle of mercury